THE ASTROPHYSICAL JOURNAL, 428:654–669, 1994 June 20

PHOTOEVAPORATION OF DISKS AROUND MASSIVE STARS AND APPLICATION TO ULTRACOMPACT H II REGIONS

DAVID HOLLENBACH
MS 245-3, NASA Ames Research Center, Moffett Field, CA 94035
DOUG JOHNSTONE
Astronomy Department, University of California, Berkeley, Berkeley, CA 94720
SUSANA LIZANO
Institute de Astronomia, UNAM, Apdo 70-264, Ciadad Universitaria, DF 04510, Mexico City, Mexico
AND
FRANK SHU
Astronomy Department, University of California, Berkeley, Berkeley, CA 94720
Received 1993 June 23; accepted 1993 December 21

ABSTRACT

Young massive stars produce sufficient Lyman continuum photon luminosity Φ_i to significantly affect the structure and evolution of the accretion disks surrounding them. A nearly static, ionized, isothermal 10^4 K atmosphere forms above the neutral disk for disk radii $r < r_g = 10^{15} M_1$ cm, where $M_* = 10\ M_\odot M_1$ is the stellar mass. For $r \gtrsim r_g$ the diffuse field created by hydrogen recombinations to the ground state in the photoionized gas above the disk produces a steady evaporation at the surface of the disk, and this H II gas flows freely out to the ISM (the "disk wind"). The detailed structure depends on the mass-loss rate $\dot{M}_w$ of the fast, $\gtrsim 1000$ km s^{-1}, *stellar* wind from the massive star. A critical mass-loss rate $\dot{M}_{cr}$ is defined such that the ram pressure of the stellar wind equals the thermal pressure of the H II atmosphere at r_g. In the weak stellar wind solution, $\dot{M}_w < \dot{M}_{cr}$, the diffuse photons from the atmosphere above r_g produce a photoevaporative mass-loss rate from the disk at $r \gtrsim r_g$ of order $1 \times 10^{-5} \Phi_{49}^{1/2} M_1^{1/2}\ M_\odot$ yr^{-1}, where $\Phi_i = 10^{49} \Phi_{49}$ s^{-1}. The resulting slow (10–50 km s^{-1}) ionized outflow, which persists for $\gtrsim 10^5$ yr for disk masses $M_d \sim 0.3 M_*$, may explain the observational characteristics of *unresolved*, ultracompact H II regions.

In the strong stellar wind solution, $\dot{M}_w > \dot{M}_{cr}$, the ram pressure of the stellar wind blows down the atmosphere for $r < r_g$ and allows the stellar photons to penetrate to greater radii and smaller heights. A slow, ionized outflow produced mainly by diffuse photons is again created for $r > r_g$; however, it is now dominated by the flow at r_w ($> r_g$), the radius at which the stellar wind ram pressure equals the thermal pressure in the evaporating flow. The mass-loss rate from the disk is of order $6 \times 10^{-5} \dot{M}_{w-6} v_{w8} \Phi_{49}^{-1/2}\ M_\odot$ yr^{-1}, where $\dot{M}_{w-6} = \dot{M}_w / 10^{-6}\ M_\odot$ yr^{-1} and $v_{w8} = v_w / 1000$ km s^{-1} is the stellar wind velocity. The resulting outflow, which also persists for $\gtrsim 10^5$ yr may explain many of the more extended ($r \gtrsim 10^{16}$ cm) ultracompact H II regions. Both the weak-wind and the strong-wind models depend entirely on *stellar* parameters (Φ_i, M_*, $\dot{M}_w$) and are independent of disk parameters as long as an extended ($r \gg r_g$), neutral disk exists. We compare both weak-wind and strong-wind model results to the observed radio free-free spectra and luminosities of ultracompact H II regions and to the interesting source MWC 349.

Subject headings: accretion, accretion disks — H II regions — radiative transfer — stars: mass loss

1. INTRODUCTION

Ultracompact (UC) H II regions are small ($r \lesssim 10^{17}$ cm), dense ($n_e \gtrsim 10^4$ cm^{-3}), high-pressure ($nT \gtrsim 10^8$ cm^{-3} K) H II regions observed around approximately 10% of the O stars in the Galaxy (Wood & Churchwell 1989a, b). The high frequency of occurrence presents a paradox: their inferred lifetimes are of order 10% of the main-sequence life of an O star or $\sim 3 \times 10^5$ yr, but their high pressures suggest that they must be expanding at speeds greater than the sound speed $a \sim 10$ km s^{-1}, which leads to a dynamical age of $\lesssim 3000$ yr. In other words, one would expect the dense gas to quickly expand and the UC H II region to quickly disappear from view, contrary to observations.

A number of explanations of the UC H II region paradox have been proposed to date (see van Buren et al. 1990 for a summary), and we review three of the more promising ones. Reid et al. (1981) initially suggested that the ram pressure from a gravitationally infalling circumstellar cloud may provide the high pressure needed to confine the UC H II regions. This suggestion was motivated, in part, by a comparison of OH observations with radio recombination lines which seemed to indicate infalling molecular material toward the UC H II region W3(OH). More recent observations (Keto et al. 1993) of W3(OH) have determined that Stark pressure broadening effects in the recombination lines coupled with velocity and density gradients produced a frequency shift that erroneously led to the original interpretation of infall. In addition, Bloemhof, Reid, & Moran (1993) have recently measured the proper motions of the OH masers and have concluded that the OH is expanding from the central star. Theoretical analysis also rules out ram pressure confinement by infall. A balance between the ram pressure of the spherical infall and the thermal pressure of

the UC H II region is unstable. Small perturbations lead either to the runaway expansion of the H II region or to the complete "crushing" of the UC H II region by the accreting material.

Van Buren et al. (1990) propose that at least some of the UC H II regions are formed in bow shocks caused by the $v_* \sim 5$–10 km s^{-1} motion of an O star through dense ($n_0 \gtrsim 10^5$ cm^{-3}) molecular gas. In their model the UC H II region lies in a shell of material that exists at a standoff distance of $r \simeq 10^{17} n_{05}^{-1/2} v_{*6}^{-1}$ cm from the star, where $v_{*6} = v_*/10$ km s^{-1} and $n_{05} = n_0/10^5$ cm^{-3}. The shell is held in balance by the outward pressure caused by the stellar wind of the O star and the inward ram pressure of the ambient gas. Such a balance is stable, and van Buren & Mac Low (1992) have produced detailed models that provide especially attractive fits to the "cometary" UC H II regions observed by Wood & Churhwell. This class of UC H II regions makes up about 20% of all UC H II regions, and these cometary regions look very much like bow shocks. The model may have difficulty, however, in explaining *all* UC H II regions and therefore in resolving the paradox of their apparent ages with their dynamical timescales. While dynamical timescales have no relevance for standing bow shocks, nevertheless tightly confined shells persist for only as long as an O star moves at high speed through dense gas. Molecular cores have the required densities, but their observed typical sizes of $\sim$0.1 pc (Myers et al. 88; Tatematsu et al. 1993) mean that the speeding O stars traverse them typically in 10^4 yr. It also seems unlikely that a high fraction of O stars should be moving so rapidly with respect to the dense molecular gas out of which they presumably formed.

Tenorio-Tagle and coworkers (e.g., Tenorio-Tagle 1979; Yorke, Tenorio-Tagle, & Bodenheimer 1983) have suggested that some UC H II regions may be "champagne" H II regions. In these models the photoevaporation of dense molecular gas with a nonspherically symmetric distribution around the star leads to an off-centered UC H II region. A one-dimensional density gradient, for example, leads to the "blowout" of the H II gas in the low-density direction and the pressure confinement in the high-density direction. In such a case, the Strömgren radius in the confinement direction expands relatively slowly as material photoevaporates from the dense neutral gas and escapes toward and past the ionizing star. Van Buren et al. (1990) have pointed out a problem in such models, if they are to explain all UC H II regions: they do not produce the limb brightening seen in some cometary configurations.

We propose that many UC H II regions are formed by the photoionization and photoevaporation of neutral accretion disks which orbit O stars for their first $\sim 10^5$ yr of main-sequence lifetime. In this model, the dense, ionized gas does expand away from the star, but *new* dense plasma is photoevaporated (and photoionized) from the neutral disk reservoir to replace it. A disk model follows naturally from current paradigms of star formation in which the gravitational collapse of a rotating cloud leads to the formation of a protostar with an orbiting circumstellar (accretion) disk. Considerable observational evidence has accumulated for the existence of these disks around low-mass stars, including the observation of infrared and ultraviolet excesses and spectra indicative of inner disk geometry (see Hillenbrand et al. 1992 for a recent review of these observations), blueshifted emission from protostellar winds indicative of disk obscuration of the redshifted component (Edwards et al. 1987; Hartmann & Raymond 1989 and references therein), and millimeter and submillimeter emission from the outer regions of the disks (e.g., Beckwith et al. 1990; Beckwith & Sargent 1993). Around low-mass stars, the disks are observationally inferred to be of size $r_d \sim 10^2$ AU and mass $M_d \sim 10^{-2}$ to 10^{-1} $M_\odot$. Recently, Beckwith & Sargent (1993) have analyzed isotopic emission from the $J = 1$–0 transition of CO and have concluded that around several T Tauri stars, the low-density portions of their disks may extend to at least 400 AU. Hillenbrand et al. (1992) have modeled the infrared emission from higher mass Ae and Be stars as arising from larger and more massive disks than low-mass pre–main-sequence stars. We notice, however, that this interpretation has been questioned by Hartmann, Kenyon, & Calvet (1993), who claim that infalling envelopes give a better solution than large massive disks for the large infrared excesses of Herbig Ae and Be stars. Despite this caveat, we anticipate that initial disk masses will continue to increase as a function of stellar mass into regions of OB star formation.

Numerous theoretical collapse calculations also show that disk formation is a highly likely outcome of the collapse of the core of a molecular cloud, due to the angular momentum in the dense molecular cloud undergoing gravitational collapse (Cassen & Moosman 1981; Terebey, Shu, & Cassen 1984; Bodenheimer, Yorke, & Laughlin 1993; Boss & Tscharnuter 1993 and references therein). In many models, most of the infalling gas from the molecular cloud falls onto the circumstellar disk, and the protostar grows due to accretion *through the disk*. The accretion disk becomes gravitationally unstable in a global sense when it reaches a mass $\simeq 0.3 M_*$, where M_* is the mass of the central protostar (Shu et al. 1990). This instability could cause significant angular momentum transfer and rapid accretion through the disk onto the star. Thus, during the collapse of the cloud core, the disk mass may be maintained close to the value $0.3 M_*$. Correspondingly, when infall ceases and the disk mass falls below the critical value, disk accretion onto the star may rapidly decline, and other mechanisms (such as photoevaporation) may disperse the remaining gas and dust.

It therefore seems quite likely that thin, neutral disks of size $r_d \gtrsim 10^{15}$–10^{16} cm and mass $M_d \simeq 0.3 M_* \simeq 3$–15 $M_\odot$ exist around massive stars early in their history. As accretion proceeds, massive stars rapidly reach the main sequence and become more (self-) luminous than their accretion luminosity. The effective temperature of the growing star ($M_* \gtrsim 10$ $M_\odot$) quickly exceeds $T_{\rm eff} \gtrsim 20{,}000$ K, and the Lyman continuum photon luminosity Φ_i becomes quite significant, $\Phi_i \gtrsim 10^{47}$ photons s^{-1}. For example, a 20 $M_\odot$ O7V star has $\Phi_i \simeq 10^{48}$ photons s^{-1} and $T_{\rm eff} \simeq 35{,}000$ K (Pottasch, Wesselius, & van Duinen 1979; Maeder & Meynet 1987; J. Simpson & R. Rubin 1993, private communication).

In our weak stellar wind model, discussed in §§ 2 and 3, the ionizing photons maintain above the thin neutral disk an ionized H II "atmosphere" of isothermal ($T \simeq 10{,}000$ K) plasma out to characteristic radius $r_g \sim 10^{15}$ cm in the disk, where the sound speed $a \sim 10$ km s^{-1} is equal to the escape speed from the orbiting disk. A "weak" stellar wind is defined as one in which the ram pressure of this $\gtrsim 1000$ km s^{-1} wind at r_g is less than the thermal pressure of the base H II atmosphere. Weak stellar winds have no significant effect on the atmosphere at r_g. Beyond r_g, a Lyman-continuum-induced ionized flow (the "disk wind") with characteristic speed $v_f \gtrsim a$ is produced, providing a steady photoevaporating mass loss $\dot{M}_{\rm dw}$ from the outer disk. The ionized plasma above the disk is maintained both by direct photons from the star and by the diffuse photons caused by the recombinations to the ground

state of the hydrogen and helium ions in the plasma. The upper atmosphere is ionized by direct photons, the lower atmosphere by diffuse photons. The flow beyond r_g is dominated by the diffuse photons produced by recombinations in the atmosphere at $r \sim r_g$.

Previous investigators have treated the photoevaporation of disks around massive stars with weak stellar winds, but none as self-consistently as the work presented here. Bally & Scoville (1982) pointed out the importance of the diffuse field in modeling S106, but they ignored the region $r < r_g$ and did not find a steady flow solution. Yorke (1993) and Yorke & Welz (1993) have used a numerical code to treat the hydrodynamics of photoevaporation in more detail, but their radiative transfer scheme ignores the diffuse field which we find to be dominant.

In the strong stellar wind model described in §§ 4 and 5, the wind ram pressure blows the atmosphere down for $r < r_g$ and allows Lyman continuum photons to penetrate to larger radii. This produces larger evaporating fluxes at large radii than the weak wind case. A new characteristic radius r_w ($> r_g$) emerges where the stellar wind ram pressure equals the thermal pressure in the *flow or disk wind.*

In both the strong and weak stellar wind models, the flow is generally "recombination limited," which means that most Lyman continuum photons are expended *maintaining* ionization in the flow, and only a small fraction are utilized to create the mass flux from the neutral/ionized interface at the disk surface. The mass-loss rate $\dot{M}_{dw}$ in the disk wind is then proportional to $\Phi^{1/2}$, and much of the mass loss occurs at $r \sim r_g$ for the weak stellar wind case and $\sim r_w$ for the strong stellar wind case. We will find that both the strong-wind and weak-wind models depend only on the *stellar* parameters (Φ_i, M_*, $\dot{M}_w$), and not on the disk parameters as long as the disk is radially extended ($r \gg r_g$) and has an ample supply of material. We discuss the validity of the model assumptions in § 6 and Appendix A.

We apply our results to H II regions in § 7, and find good agreement with emission measures, spectra, and spatial extent of UC H II regions. In addition, the steady-state outflow in this model results in the persistence of such UC H II regions for the lifetime of the photoevaporating disk, which is $\sim 10^5$ yr for disk masses of $\sim 3\ M_\odot$ and $\Phi_{49} \sim 1$. This therefore resolves the apparent disparity between the UC H II region lifetime and the dynamic age. We summarize our results in § 8.

2. PHOTOEVAPORATION MODEL: WEAK STELLAR WIND CASE

2.1. *Model Assumptions*

We assume that the stellar disk, which is being photoevaporated, can be represented by a spatially thin, neutral disk which is optically thick to Lyman continuum photons. We will show that the diffuse field generally dominates the production of the ionized atmosphere and the photoevaporating flow. In such a case, the exact shape of the disk is unimportant (e.g., "shadowing" effects are eliminated and the disk need not be razor thin), as long as the major part of the atmosphere can be illuminated by starlight. We justify the approximation that the disk is spatially thin and optically thick a posteriori in Appendix A.

We assume ionization equilibrium and an H II region temperature of 10^4 K, arising from a balance between heating, due primarily to incident ionizing photons, and cooling, due primarily to forbidden line radiation. We verify a posteriori in Appendix A the assumption of ionization and thermal equilibrium.

The dynamical evolution of the atmosphere is modeled by assuming that inside the gravitational radius, r_g, the atmosphere is static. Beyond r_g, where the thermal speed is greater than the escape speed, the photoevaporated material flows from the disk at the sound speed of the ionized hydrogen.

The central star is replaced by two point sources located above and below the plane of the disk. The location of the point source above the plane of the disk was calculated such that for an unattenuating atmosphere, the same amount of flux would reach the disk from either the point source or the extended star. The point sources are located at heights, $h = \pm 0.424 R_*$, where R_* is the stellar radius. Figure 1 schematically depicts the model in one hemisphere. The central star could have been represented by a point source at the origin; however, placing it above the plane allows us to determine the effect of the direct flux incident on the disk and to show that the diffuse flux dominates the direct flux in forming the atmosphere and the mass outflow. Because the diffuse flux is dominant, the neutral disk need not be infinitely thin, but rather the weak condition $z_n/r \lesssim 0.5$ need only apply, where z_n is the height of the neutral disk. We discuss this further below and in Appendix A.

We have ignored the effect of dust in the atmosphere. Attenuation of Lyman continuum photons is entirely due to the trace amounts of recombined hydrogen atoms in the H II plasma. Dust would cause a greater amount of attenuation to take place within the atmosphere and thus reduce the intensity

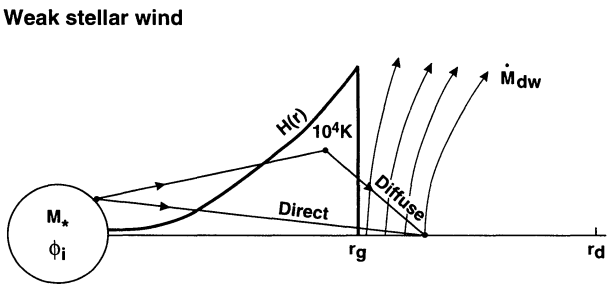

FIG. 1*a*

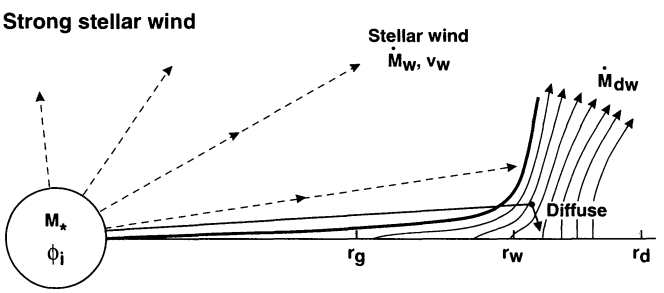

FIG. 1*b*

FIG. 1.—(*a*) Schematic for the weak stellar wind model for a star of mass M_* and Lyman continuum photon luminosity Φ_i. Inside r_g an ionized 10^4 K atmosphere forms with scale height $H(r)$. Diffuse Lyman continuum photons from recombinations in the atmosphere at $\sim r_g$ cause material to evaporate beyond r_g. The disk extends to r_d. (*b*) Schematic for the strong stellar wind model for a star with a mass-loss rate $\dot{M}_w$. Material evaporates beyond r_g, but the dominant flow is from r_w, where the stellar wind ram pressure equals the thermal pressure of the ionized flow of the disk. Diffuse photons still dominate the photoevaporation.

of the flux from the central star. This in turn would lower the electron density in the atmosphere and mass outflow regions, and subsequently lower the photoevaporated mass-loss rate. Radiation pressure on the dust might also affect the dynamical evaporation evolution of the outflow region, accelerating the dust and dragging the gas to speeds greater than the sound speed; this mechanism promotes photoevaporation from the disk surface. We discuss the quantitative effects of dust grains on the photoevaporative flow in § 6.

2.2. *Model Parameters*

In the weak stellar wind case the photoevaporating disk models require only two parameters, the stellar mass M_* and the ionizing photon luminosity Φ_i, to specify them uniquely. The radius R_* of the central star does not affect the solutions because the diffuse field dominates and most evaporation occurs for $r \gg R_*$. All that is required of the neutral disk is that it exists and extends to $r \gg r_g$.

In UC H II regions, the mass of the central star is typically in the range $15\ M_\odot < M_* < 65\ M_\odot$. Masses in this range yield an ionizing Lyman continuum luminosity of $3 \times 10^{47}\ s^{-1} < \Phi_i < 3 \times 10^{49}\ s^{-1}$ based on models by Maeder & Meynet (1987). The corresponding stellar radii, R_*, are of order 3×10^{11}–7×10^{11} cm. Table 1 lists the stellar parameters adopted for various stars chosen to span this range of Φ_i, M_*, and R_*.

2.3. *Characteristic Length Scales*

Three length scales emerge in the weak wind model. The gravitational radius r_g marks the boundary between the static atmosphere ($r < r_g$) and the photoevaporating ionized plasma $r > r_g$. The scale height H, a function of disk radius, defines the height (z) dependence of the atmospheric density for $r \leq r_g$. The characteristic disk radius, r_*, is the distance at which the scale height is identical to the effective radius of the star, h.

The gravitational radius, r_g, can be found by equating the sound speed $a = (kT/m_{\rm II})^{1/2}$ and the orbital velocity, $v_o = (GM_*/r)^{1/2}$. The mean mass per particle $m_{\rm II}$ in the H II gas is taken to be 1.13×10^{-24} g in our models. Thus,

$$r_g = \frac{GM_*}{a^2} \approx 10^{15} M_1 \text{ cm}\ , \tag{2.1}$$

where $M_1 = M_*/10\ M_\odot$.

The scale height of the ionized atmosphere, $H(r)$, is determined by solving the equations of hydrostatic equilibrium for an isothermal atmosphere. Given M_*, the mass of the central star, and T, the temperature of the isothermal atmosphere, the scale height is

$$H(r) = \left(\frac{kT}{m_{\rm II}} \frac{r^3}{GM_*}\right)^{1/2} = \left(\frac{a}{v_o}\right) r\ , \quad (H < r) \tag{2.2}$$

where k is the Boltzmann constant and G is the gravitational constant. The scale height increases outward along the disk, following the power-law form $H(r) \propto r^{3/2}$. The scale height may be written more simply in terms of r_g

$$H(r) = r_g \left(\frac{r}{r_g}\right)^{3/2}\ , \quad (H \leq r_g) \tag{2.3}$$

where we note that the scale height at the gravitational radius is $H(r_g) = r_g$. The assumption of $H \ll r$ leads to a separable solution for the electron density distribution,

$$n_e(r, z) = n_0(r) \exp\left(-z^2/2H^2\right)\ , \quad (r < r_g)\ , \tag{2.4}$$

where $n_0(r)$ is the electron density at the base of the atmosphere.

The characteristic radius r_*, is the radius at which the scale height equals h (see Figs. 1 and 2):

$$r_* = (r_g h^2)^{1/3} \approx 5 \times 10^{12}\ M_1^{1/2} \left(\frac{R_*}{10^{12}\text{ cm}}\right)^{2/3} \text{cm}\ . \tag{2.5}$$

As they pierce the atmosphere, ray paths from the central source that reach the midplane at $r < r_*$ suffer attenuation over $H(r)/\sin(\theta)$, where $\theta \sim h/r$ is the angle of incidence. Therefore, for $r < r_*$, the attenuation pathlength increases proportional to $r^{5/2}$. On the other hand, ray paths that reach the midplane at $r > r_*$ suffer attenuation over a pathlength, approximately $r - r_*$. This difference produces a change in the r dependence of $n_0(r)$ at r_*.

2.4. *Radiative Transfer Model*

2.4.1. *The Static Region, $r < r_g$*

The density distribution of the ionized hydrogen atmosphere determines the attenuation of the UV photon flux from the central star and the production of diffuse Lyman continuum photons via recombinations to the ground state in the atmosphere. It thereby regulates the amount of ionized hydrogen that is able to escape from beyond r_g. Since the z dependence of the electron density distribution is known (eq. [2.4]), the problem is solved once $n_0(r)$ is determined. The basic equation of $n_0(r)$ requires that all Lyman continuum photons are absorbed by recombined hydrogen atoms before reaching the midplane.

The diffuse ionizing radiation field is produced by the nearly one in three recombinations that goes directly to the ground

TABLE 1

STELLAR MODELS

Model	M_* ($M_\odot$)	Φ_i (s^{-1})	T_* (10^4 K)	R_* (10^{11} cm)	L ($L_\odot$)	$\dot{M}_w$ ($M_\odot$/yr)	Wind
1.....	16.8	3.75 (47)	3.3	3.48	2.68 (4)	0	Weak
2.....	25.6	3.40 (48)	3.9	4.39	8.32 (4)	0	Weak
3.....	65.0	3.78 (49)	5.0	7.27	6.15 (5)	0	Weak
4.....	16.8	3.75 (47)	3.3	3.48	2.68 (4)	4.8 (−8)	Standard
5.....	25.6	3.40 (48)	3.9	4.39	8.32 (4)	3.6 (−7)	Standard
6.....	65.0	3.78 (49)	5.0	7.27	6.15 (5)	3.5 (−6)	Standard
7.....	65.0	3.78 (49)	5.0	7.27	6.15 (5)	7.0 (−6)	Strong

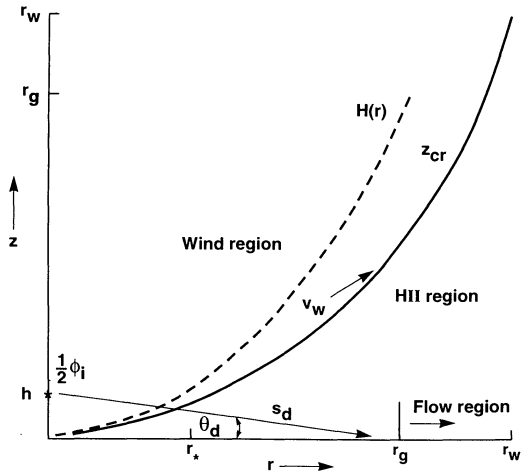

FIG. 2.—Schematic showing the height of the ionized disk atmosphere with radius for the weak (*dashed line*) and strong (*solid line*) stellar wind models. Note that the effect of the strong stellar wind is to reduce the height of the atmosphere. The solid line indicates the interface where the normal component of the stellar wind ram pressure equals the thermal pressure of the disk H II gas. The free flowing stellar wind is to the left of the solid line; the H II gas (either atmosphere for $r < r_g$ or "disk-wind" for $r > r_g$) is to the right. Also shown is the grazing path which direct radiation from the central star must take to intercept the disk at large radii.

level. While the direct flux incident on the disk at large radii suffers great attenuation as it passes through high-density hydrogen particularly near $r, z \approx r_*, h$, the diffuse flux from the outer atmosphere, $r, z \sim r_g, r_g$ avoids the attenuation at r_*, h as it shines vertically downward onto the disk, producing a high value of $n_0(r_g)$ (see Figs. 1 and 2). Thus, the diffuse flux plays the dominant role in determining the density of the atmosphere at large distances, $r \gg r_*$.

Properly solving the radiative transfer, including the diffuse photons, would require an iterative approach because all points of the atmosphere are intimately coupled. To simplify the computation we note that, for a power-law density function $n_0(r) \propto r^{-\beta}$, the diffuse flux onto the disk at r is dominated by the atmosphere above r as long as $0.75 < \beta < 1.75$. Therefore, we adopt the Eddington approximation to treat the diffuse radiation field that determines $n_0(r)$ as an eigenvalue problem at each r, and then self-consistently check to see if the derived value of β lies within the limits that justify our assumption. In essence, we reduce the complicated three-dimensional radiative transfer problem to a "three stream" approximation, with one-dimensional fluxes incident at each atmospheric position from three directions: the star, and directly upwards and downwards.

The differential equations governing the upward $F_u(r, z)$, and downward, $F_d(r, z)$, diffuse fluxes at any disk radius r are

$$\frac{d}{dz} F_u = -n_H(r, z)\sigma F_u + \frac{1}{2} n_e^2(r, z)k_1 , \tag{2.6a}$$

$$\frac{d}{dz} F_d = +n_H(r, z)\sigma F_d - \frac{1}{2} n_e^2(r, z)k_1 , \tag{2.6b}$$

where k_1 is the recombination rate coefficient to the ground state, and σ is the photoionization cross section of atomic hydrogen, and where we have adopted the sign convention that the downward flux F_d is positive. The first term on the right-hand side of equation (2.6) is the attenuation term due to the trace amounts of atomic hydrogen at density n_H; the second term is the source term due to recombination to the ground state.

The stellar flux F_* is given by the differential equation

$$\frac{1}{s^2}\frac{d}{ds} s^2 F_*(s, \theta) = n_H(r, z)\sigma F_*(s, \theta) , \tag{2.7}$$

where s is the ray path length and θ is the angle the ray makes to the disk (so that $z = h - s \sin\theta$ and $r = s \cos\theta$).

The ionization balance equation is

$$n_H(r, z)\sigma(F_* + F_u + F_d) = n_e^2(r, z)\alpha_1 , \tag{2.8}$$

where α_1 is the total recombination rate coefficient.

One seeks the eigenvalue $n_0(r)$ that allows the stellar and diffuse fluxes to satisfy the boundary conditions $F_u = F_d = F_*(s_d, \theta_d) = 0$ at $z = 0$, where $s_d = r/\cos\theta_d$ is the path from the "half star" at $r = 0$, $z = h$ to the disk at r, $z = 0$; $F_d \to 0$ at $z \gg H$; and $F_*(R_*, \theta) = \Phi_i/(8\pi R_*^2)$ is the stellar flux at the stellar surface (the factor of $\frac{1}{2}$ arises since half the photons are emitted above and below the plane). In practice, this procedure is accomplished by advancing the solution for $n_0(r)$ outwards from the stellar surface. Our numerical procedure calculates the direct ionization and the diffuse flux many scale heights above the surface.

2.4.2. *The Flow Region, $r > r_g$*

Beyond the gravitational radius r_g, the evaporated hydrogen from the disk is able to flow away from the central star. In this region we assume that the density is only a function of disk radius (i.e., the flow is vertical and at a constant speed a), thus $n_e(r, z \le r) = n_0(r)$ for $r > r_g$. Since material is evaporating from the disk, the boundary condition for the incident flux at the neutral/ionized interface is now the condition that the normal component of the photon flux at the base of the flow (we assume a thin neutral disk so the base is approximated as the midplane) equals the flux of proton-electron pairs liberated, that is

$$\frac{h}{r} F_*(r, \theta_d) + F_d(r, z = 0) = an_0(r) , \tag{2.9}$$

where we have approximated $s_d \simeq r$ and $\sin\theta_d \simeq h/r$. The first term of the left-hand side of equation (2.9) represents the normal component of the direct photon flux from the star; the second term is the diffuse photon flux.

As mentioned above, the attenuation of the direct flux from the central star is formidable along rays that intersect the disk at $r \gg r_*$. Since the normal flux is necessary in determining the amount of material flowing, the grazing angle between the incident direct flux beam and the disk reduces the efficiency of direct flux-induced evaporation further. The diffuse flux from the enormous reservoir of atmosphere above r_g, coupled with less attenuation along the path from $r, z \approx r_g, r_g$ to the disk and the better angle of incidence with the midplane (see Figs. 1 and 2), reinforce the importance of the diffuse flux in determining the amount of evaporation of hydrogen from the disk. Because the diffuse flux dominates the solution for $n_0(r)$, the grazing angle between the direct flux and the neutral disk becomes irrelevant, and the neutral disk need not be infinitely thin. The neutral disk is effectively thin as long as $z_n/r \lesssim 0.5$, so that a substantial ionized atmosphere may exist (and produce diffuse photons) at $r \lesssim r_g$. We have verified this numerically (see Appendix A).

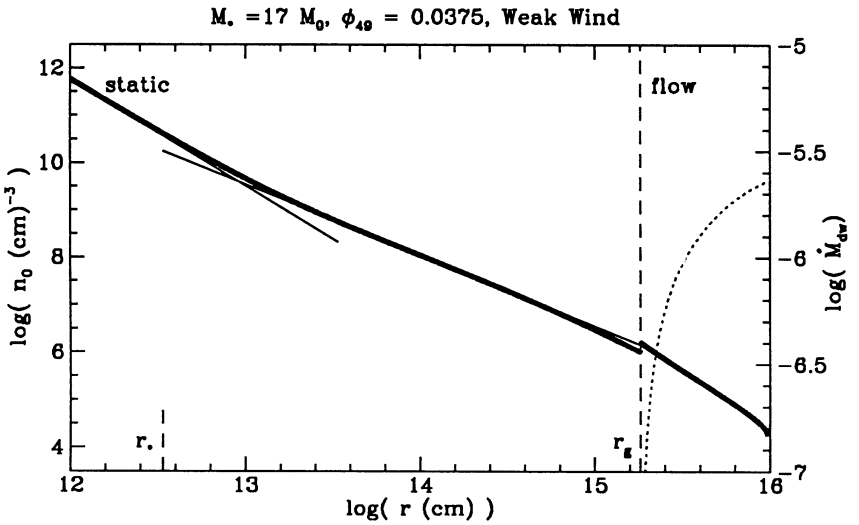

FIG. 3.—Numerical solution for the base number density of electrons (*heavy solid line*) in the ionized atmosphere as a function of radius for a 17 $M_\odot$ star with a weak stellar wind (model 1). The dashed vertical line signifies division between the static region $r < r_g$ and the flow region $r > r_g$. The thin straight lines are the analytic solutions given in the text. The dotted curve on the right-hand side shows the cumulative mass loss due to the disk wind as a function of radius.

3. RESULTS: WEAK STELLAR WIND CASE

Figures 3–5 show the numerical solutions that have been found for the base number density n_0 of ionized hydrogen as a function of disk radius r for the weak wind models listed in Table 1, which spans $M_* = 15$–$65\ M_\odot$ and $\Phi_i = 3 \times 10^{47}$–$3 \times 10^{49}$ photons s^{-1}. Three distinct regions in the $n_0(r)$ plots are noticeable. At very small distances from the central star, $r < r_*$, $n_0(r)$ scales as $r^{-9/4}$; at intermediate radii $r_* < r < r_g$, $n_0(r) \propto r^{-3/2}$; for $r > r_g$, $n_0(r) \propto r^{-\gamma}$, where $\gamma > 2$. For $\gamma > 2$, the mass loss (and the integrated emission measure of the flow) is dominated by loss at $r \sim r_g$. The hydrogen mass-loss rate via evaporation $\dot{M}_{\rm dw}$ is

$$\dot{M}_{\rm dw} = 2m_{\rm H} v \int_{r_g}^{\infty} 2\pi n_0(r) r\, dr\ , \qquad (3.1)$$

where $m_{\rm H}$ is the mass of a proton-electron pair and the flow velocity $v = a \simeq 10$ km s^{-1} for $r > r_g$. Since the density distribution declines faster than r^{-2}, eq. (3.1) can be written

$$\dot{M}_{\rm dw} = 4\pi(\gamma - 2)^{-1} m_{\rm H} v n_0(r_g) r_g^2\ . \qquad (3.2)$$

Table 2 lists the evaporative mass-loss rates $\dot{M}_{\rm dw}$ determined from inserting the numerical solutions for $n_0(r)$ into equation (3.1). $\dot{M}_{\rm dw}$ scales as $\Phi_i^{1/2} M_*$ for the weak stellar wind cases for reasons discussed below.

These numerical results can be understood through approximate analytic solutions to $n_0(r)$. It is illustrative to consider a one-dimensional problem in which a source of Lyman continuum flux F_i irradiates a surface a distance l away, creating photoevaporated flux $n_0 v$ of ionized particles. Gravitational fields are assumed to be negligible. The particle flux velocity v, in such a case, is of order the sound speed a of the 10,000 K photoionized plasma and, assuming constant velocity flow, the density n_0 is constant between the surface and the source. The ionized flux is absorbed by recombined hydrogen atoms in the flow between the surface and the source and by the creation of

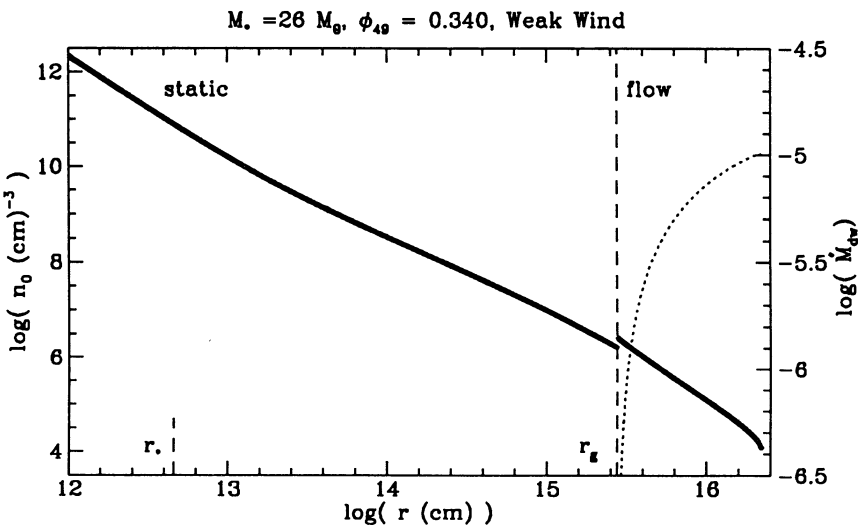

FIG. 4.—Similar numerical solution as in Fig. 3 for a 26 $M_\odot$ star with a weak wind (model 2)

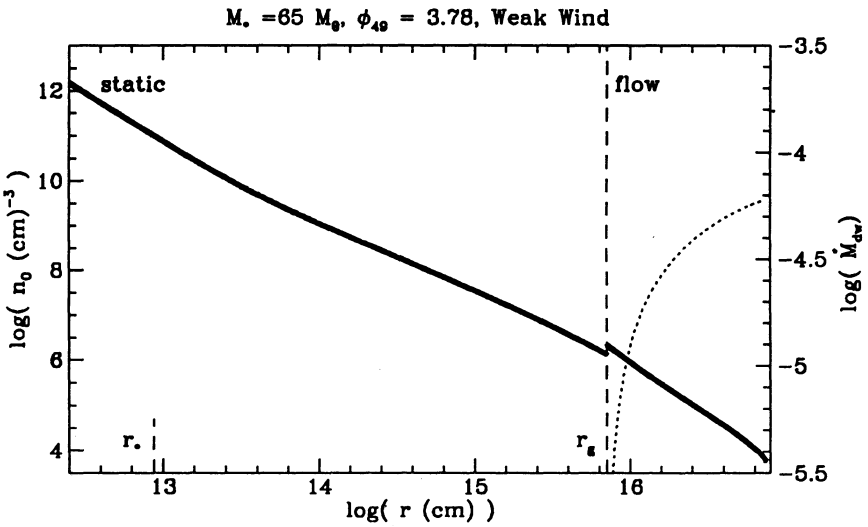

FIG. 5.—Similar numerical solution as in Fig. 3 for a 65 $M_\odot$ star with a weak wind (model 3)

new ion pairs at the surface (the ionized/neutral interface). This can be expressed as

$$F_i = \alpha_2 n_0^2 l + n_0 v \,, \tag{3.3}$$

where α_2 is the recombination coefficient to all states except the ground state (case B). The first term on the right-hand side expresses the fact that every case B recombination in the flow between the surface and the source results in an atom that quickly absorbs a Lyman continuum photon and is reionized. If this term dominates, the flow is "recombination limited," as most of the photon flux is used to reionize recombined atoms in the flow. In this case,

$$n_0,\ \dot{M}_{\rm dw} \propto F_i^{1/2} \propto \Phi_i^{1/2} \,. \tag{3.4}$$

On the other hand, if the second term on the right-hand side of equation (3.3) dominates, then the flow is "particle flux limited," and

$$n_0,\ \dot{M}_{\rm dw} \propto F_i \propto \Phi_i \,. \tag{3.5}$$

Here, every photon emitted by the source creates a new proton-electron pair, and the mass loss goes directly as the photon luminosity. For massive stars the flows are predominantly recombination limited, and n_0 and $\dot{M}_{\rm dw}$ are proportional to $\Phi_i^{1/2}$.

We can use the simple one-dimensional equation (3.3) to analytically solve the $r < r_*$ case for $n_0(r)$. Inside r_*, the diffuse field is not significant because the stellar flux shines downward through the atmosphere and suffers similar attenuation as the diffuse field. For $r \ll r_g$, the flow is negligible (we assume $v = 0$), and the atmosphere is recombination limited. Equation (3.3) can be rewritten to approximate this situation

$$\frac{\Phi_i}{8\pi r^2} = \alpha_2 n_0^2 \left(\frac{r}{h}\right) H \,, \tag{3.6}$$

where H is the scale height and the term in parentheses corrects for the obliquity of the effective pathlength caused by the grazing angle of the stellar photons on the disk surface. Using equation (2.3), we derive the electron density at the base (the ion/neutral interface)

$$n_0 = \frac{r_g^{1/4} h^{1/2} \Phi_i^{1/2}}{(8\pi\alpha_2)^{1/2} r^{9/4}} \tag{3.7}$$

in the static atmosphere close to the star ($r < r_*$). Extracting the parameter dependence from this analytic approximation, but replacing the analytic coefficient with a best fit to the more accurate numerical solutions, we obtain

$$n_0 = 1.2 \times 10^{10} M_1^{1/4} h_{11}^{1/2} \Phi_{49}^{1/2} r_{13}^{-9/4} \ {\rm cm}^{-3} \quad (r < r_*) \,, \tag{3.8}$$

where $h_{11} = h/10^{11}$ cm, $r_{13} = r/10^{13}$ cm, and $\Phi_{49} = \Phi_i/10^{49}$ s^{-1}. The analytic solution (3.7) exactly reproduces the observed dependences of n_0 on r, M_*, h, and Φ_i, and the analytic numerical coefficient is within order unity of the numerical value.

In the region $r_* < r < r_g$, the diffuse flux determines $n_0(r)$. Although more rigorous analytic solutions may be found, a simple dimensional analysis provides the clearest insights and matches the numerical results. A density profile $n_0(r)$ sets up

TABLE 2

MODEL RESULTS

Model	M_* ($M_\odot$)	Φ_{49} (10^{49} s^{-1})	$\dot{M}_{w-6}$ (10^{-6} $M_\odot$/yr)	$\dot{M}_{dw-5}$ (10^{-5} $M_\odot$/yr)	r_g (cm)	r_w (cm)	$n_0(r_g)$ (cm^{-3})	$n_0(r_w)$ (cm^{-3})
1.....	16.8	3.75 (−2)	0	3.2 (−1)	1.8 (15)	...	1.4 (6)	...
2.....	25.6	3.40 (−1)	0	1.2 (0)	2.8 (15)	...	2.2 (6)	...
3.....	65.0	3.78 (0)	0	6.4 (0)	7.1 (15)	...	1.8 (6)	...
4.....	16.8	3.75 (−2)	4.0 (−2)	3.2 (−1)	1.8 (15)	1.3 (15)	1.4 (6)	...
5.....	25.6	3.40 (−1)	3.6 (−1)	3.5 (0)	2.8 (15)	5.3 (15)	2.2 (6)	9.3 (5)
6.....	65.0	3.78 (0)	3.5 (0)	1.0 (1)	7.1 (15)	4.1 (16)	1.8 (6)	1.5 (5)
7.....	65.0	3.78 (0)	7.0 (0)	2.0 (1)	7.1 (15)	1.4 (17)	1.8 (6)	2.8 (4)

such that the Strömgren condition applies at each radius, or

$$\tfrac{4}{3}\pi r^3 \alpha_2 n_0^2(r) = \Phi_i \,, \tag{3.9}$$

$$n_0(r) = \left(\frac{3\Phi_i}{4\pi\alpha_2 r^3}\right)^{1/2} , \tag{3.10}$$

valid for $r_* < r < r_g$. The numerical results slightly change the constant coefficient to obtain

$$n_0(r) = 1.8 \times 10^7 \Phi_{49}^{1/2} r_{15}^{-3/2} \text{ cm}^{-3} \quad (r_* < r < r_g) \,, \tag{3.11}$$

where $r_{15} = r/10^{15}$ cm.

The $r^{-3/2}$ dependence can be understood in a qualitative way. If the density declined more rapidly with distance, the atmosphere would be density bounded, and thus substantial amounts of ionizing radiation would penetrate, raising the electron density in the outer regions. On the other hand, if the density declined more slowly, the atmosphere would become ionization bounded, and the ionizing flux would be severely attenuated. Since ionizing flux is required to maintain the atmosphere in the outer region, the electron density in these regions would therefore decline. Note that this dimensional analysis does not require an infinitely thin disk, but rather $z_w/r \lesssim 1$.

For $r > r_g$, the mounting attenuation of stellar photons causes $n_0(r)$ to drop more steeply, $n_0(r) \propto r^{-\gamma}$ where $\gamma > 2$. With such a steep dependence, the diffuse flux at $r > r_g$ derives from recombinations in the atmosphere at r_g. In such a case, it can be shown analytically that

$$n_0(r) = n_0(r_g)\left(\frac{r}{r_g}\right)^{-5/2} \quad (r > r_g) \,, \tag{3.12}$$

valid as long as the flow is recombination limited. Numerically, we obtain $\gamma \simeq 2.5$, but it should be noted that the numerical results assume that it is the *overhead* diffuse flux that dominates rather than the diffuse flux from r_g. Substituting $n_0(r_g)$ from equation (3.10) into equation (3.12) and then integrating equation (3.1) to determine $\dot{M}_{\rm dw}$, we obtain the analytic approximation

$$\dot{M}_{\rm dw} = \frac{(12\pi)^{1/2}}{(\gamma - 2)} m_{\rm H} a \left(\frac{\Phi_i r_g}{\alpha_2}\right)^{1/2} . \tag{3.13}$$

Adjusting the numerical coefficient slightly to fit the more exact numerical results, we obtain

$$\dot{M}_{\rm dw} = 1.3 \times 10^{-5} \Phi_{49}^{1/2} M_1^{1/2} \; M_\odot \text{ yr}^{-1} \,. \tag{3.14}$$

Equations (3.8), (3.11), (3.12), and (3.14) therefore provide a complete "analytic" solution to the electron density structure and mass-loss rates in photoevaporating disks illuminated by central stars with Lyman continuum photon luminosities Φ_i and weak stellar winds.

4. PHOTOEVAPORATION MODEL: STRONG STELLAR WIND CASE

4.1. *Model Assumptions*

We make the same assumptions as in the weak wind model (see § 2.1) with the additional assumption that the stellar wind forms a laminar slip surface on the top of the atmosphere for $r < r_g$ and of the photoevaporating flow for $r > r_g$. The boundary z_w between wind and H II plasma is determined by setting the normal component of the stellar wind ram pressure equal to the thermal pressure of the H II gas (see Fig. 2). The "slip" assumption means that we ignore the flux of H II gas originating from $r < r_g$ which will be entrained in the shocked wind flow and carried outwards to escape. The electron density n_e as a function of height z is given by equation (2.4) for $z < z_w$, and by $n_e = 0$ for $z > z_w$ (i.e., we ignore the low electron density of the ionized, free-flowing stellar wind[1]).

4.2. *The Critical Mass-Loss Rate $\dot{M}_{\rm cr}$ in the Stellar Wind: Strong versus Weak Winds*

In the case of a weak stellar wind, the photoevaporation of disk material is dominated by the diffuse flux of Lyman continuum photons produced by the recombining H II atmosphere above the disk at r_g. Therefore, a critical momentum rate $\dot{M}_w v_w$ in the stellar wind is defined such that the ram pressure in the wind is equal to the thermal pressure of the lower atmosphere at $r = r_g$. Because the wind speed v_w only varies by a factor of about 3 (1000 km s^{-1} to 3000 km s^{-1}) for most early-type stars, whereas $\dot{M}_w$ can range over several decades (e.g., van Buren 1985), we reduce the critical momentum rate to a critical mass-loss rate $\dot{M}_{\rm cr}$. For $\dot{M}_w < \dot{M}_{\rm cr}$, the stellar wind may affect the inner ($r \ll r_g$) atmosphere and the upper (higher than one scale height) atmosphere at larger radii; however, the bulk of the atmosphere at r_g is preserved, and the solution for the photoevaporating flow at $r \gtrsim r_g$ reduces to the "weak-wind" solution. For $\dot{M}_w > \dot{M}_{\rm cr}$, the ram pressure of the stellar wind blows down the atmosphere at r_g. In this case, more direct ionizing photons from the star penetrate to greater radii and lower heights, resulting in enhanced photoevaporation at larger disk radii.

Using equation (3.11) to determine the thermal pressure at r_g, we find that $\dot{M}_{\rm cr}$ is given

$$\dot{M}_{\rm cr} = 1.0 \times 10^{-7} \Phi_{49}^{1/2} M_1^{1/2} v_{w8}^{-1} \; M_\odot \text{ yr}^{-1} \,, \tag{4.1}$$

where v_{w8} is the stellar wind speed in units of 1000 km s^{-1}. Mass-loss rates from O-type stars generally exceed this value (van Buren 1985) so that the "strong wind" case typically applies to these stars. On the other hand, stars later than about B0 often have $\dot{M}_w < \dot{M}_{\rm cr}$ so that the later type stars may more generally be considered "weak wind" candidates.

4.3. *Model Parameters*

In the strong wind case, $\dot{M}_w > \dot{M}_{\rm cr}$, three parameters specify the models: M_*, Φ_i, and $\dot{M}_w$ (we ignore the dependence on v_w because of its small range). Although there is considerable scatter, Φ_i and $\dot{M}_w$ are observed to be correlated (e.g., van Buren 1985). Using the correlation noted by van Buren along with the stellar models of Panagia (1973), we derive the following approximate relation for B0V-O4V stars:

$$\dot{M}_{w-6} \simeq \Phi_{49}^{0.94} \,, \tag{4.2}$$

where $\dot{M}_{w-6} = \dot{M}_w/10^{-6} \; M_\odot \text{ yr}^{-1}$. We emphasize that any individual O star may deviate by as much as a factor of 10 from this overall correlation. However, equation (4.2) can be used to crudely reduce the three basic parameters to two. The stellar mass-loss rates, from equation (4.2), typically range from 3×10^{-8} to 3×10^{-6} $M_\odot$ yr^{-1} for the early-type stars we consider. Table 1 lists M_w along with the effective surface temperature, T_e, and the stellar luminosity, L, for model stars chosen to span the typical range of M_*, Φ_i, and $\dot{M}_w$.

[1] We also note that the ionized *stellar* wind has much too low electron densities, and therefore emission measures, and much too high velocities to provide the origin of UC H II regions.

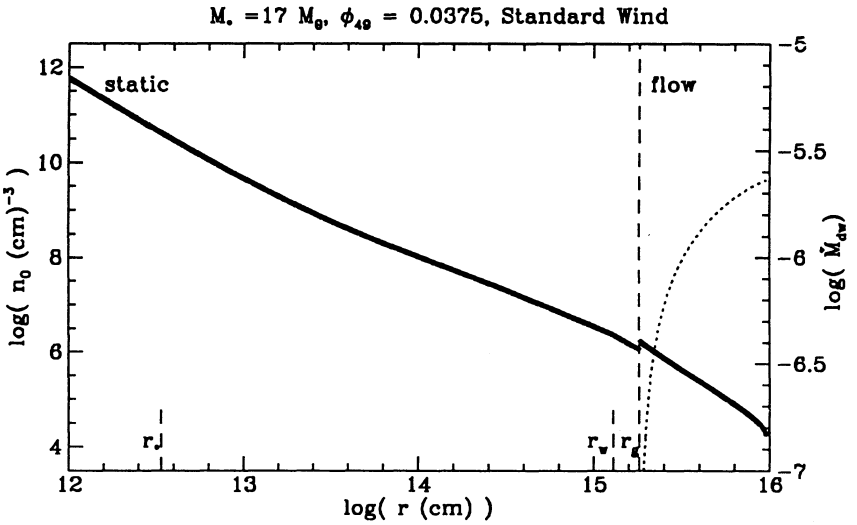

FIG. 6.—Similar numerical solution as in Fig. 3 for a 17 $M_\odot$ star with a standard wind (model 4)

The "standard wind" models are those that use relation (4.2) to set $\dot{M}_w$.

4.4. *Characteristic Lengths*

In the strong wind case a fourth characteristic length is introduced: the disk radius r_w is the distance at which the radial ram pressure of the stellar wind equals the thermal pressure of the evaporating flow. The critical disk radius r_w depends on the solution to the variation of flow density with radius described in § 5; we anticipate the results of § 5 here to set r_w:

$$r_w = 1 \times 10^{16} \dot{M}_{w-6}^2 v_{w8}^2 \Phi_{49}^{-1} \text{ cm} . \quad (4.3)$$

If we use the rough scaling (eq. [4.2]) of $\dot{M}_w$ to Φ, we obtain

$$r_w = 1 \times 10^{16} \Phi_{49}^{0.88} v_{w8}^2 \text{ cm} , \quad (4.4)$$

valid for $r_w > r_g$ or $\dot{M}_w > \dot{M}_{cr}$. To get a sense of the magnitudes of r_w and r_g, note that the $M_* = 65\ M_\odot$ standard wind case of Table 1 results in $r_g = 6.5 \times 10^{15}$ cm and $r_w = 4 \times 10^{16} v_{w8}^2$ cm. For $r_g < r < r_w$, the photoevaporating flow encounters the wind at a height $z \ll r$, and is bent into a nearly radially propagating sheet of outflow. For $r > r_w$, the photoevaporating flow propagates vertically to a height $z \sim r$, where pressure gradients bend the flow to a roughly spherically symmetric radial outflow (see Figs. 1 and 2). We have implicitly assumed that the circumstellar disks extend to radii $r > r_w$ in calculating the model results.

5. PHOTOEVAPORATION RESULTS: STRONG WIND CASE

Figures 6–8 show the numerical solutions that have been found for the base density of electrons (or hydrogen nuclei) $n_0(r)$ as a function of disk radius for the "standard wind" models listed in Table 1, which span $M_* = 15$–$65\ M_\odot$. We see in Figure 6 that the 15 $M_\odot$ model represents the borderline case $r_w \simeq r_g$ for the standard winds chosen. For $M_* < 15\ M_\odot$ the standard wind results in a weak wind solution; for $M_* > 15\ M_\odot$ the standard wind results in a strong wind solution. Figure 9 shows that the 65 $M_\odot$ case with a stronger than average wind. Figure 10 presents numerical results that show the dependence of r_w on $\dot{M}_w$ and Φ_i: $r_w \propto \dot{M}_w^2 \Phi_i^{-1}$.

The numerical results for $n_0(r)$ can be summarized as follows: $n_0(r) \propto r^{-9/4}$ for $r < r_*$ as in the weak wind case;

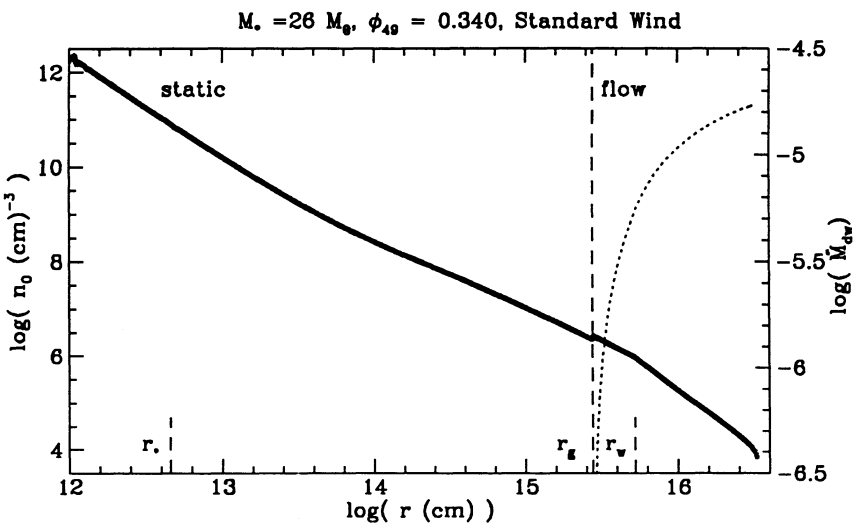

FIG. 7.—Similar numerical solution as in Fig. 3 for a 26 $M_\odot$ star with a standard wind (model 5)

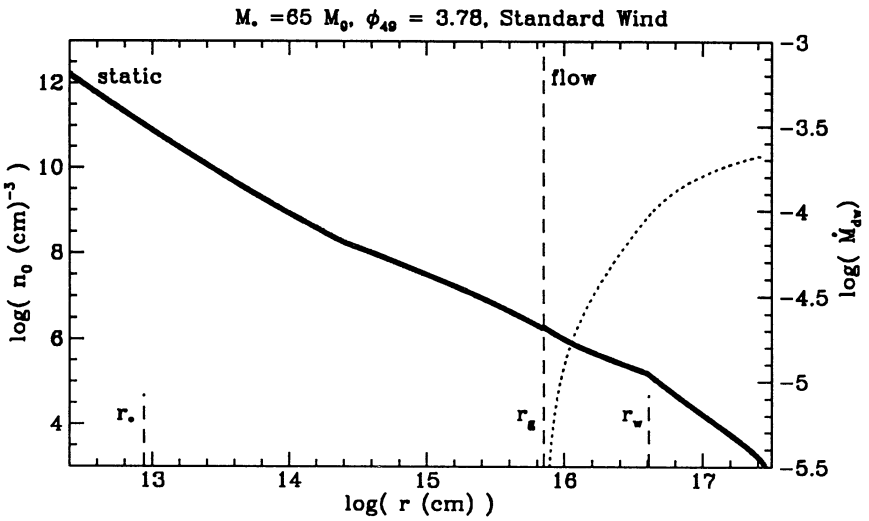

FIG. 8.—Similar numerical solution as in Fig. 3 for a 65 $M_\odot$ star with a standard wind (model 6)

$n_0(r) \propto r^{-2}$ for an intermediate region beyond r_*, but eventually the solution rises to the same $n_0(r) \propto r^{-3/2}$ solution as in the weak wind case; the $n_0(r) \propto r^{-3/2}$ solution persists further than the weak wind case (to r_w instead of r_g) and, for $r > r_w$, $n_0(r)$ rapidly declines, $n_0(r) \propto r^{-\gamma}$ with $\gamma \sim 5/2$. Such a solution implies (see eq. [3.2]) that

$$\dot{M}_{\rm dw} \simeq \left(\frac{4\pi}{\gamma - 2}\right) m_{\rm H}\, a r_w^2\, n_0(r_w)\,, \qquad (5.1)$$

or the mass-loss rate is determined by the electron density at r_w. The evaporative mass-loss rate is found from the numerical solutions to scale as $\dot{M}_w \Phi^{-1/2}$. The numerical values for the cases run appear in Table 2.

We can derive approximate analytic solutions convenient for generalizing and understanding the numerical results. For $r < r_*$, the star dominates and the analytic solution for $n_0(r)$ is the same as in the weak wind case (eq. [3.8]). In the intermediate region beyond r_*, the strong wind blows down the atmosphere, reducing the diffuse flux to insignificance. For $r > r_*$, the analytic solution to $n_0(r)$ when the direct flux from the star dominates is $n_0(r) \propto r^{-2}$. However, the atmosphere/wind boundary inevitably curves upwards, that is, its slope increases with r since it must produce a normal component of wind ram pressure to balance the thermal pressure below. Eventually, therefore, the atmosphere attains sufficient height that the diffuse flux regains its dominance and the solution to $n_0(r)$ reverts to our weak wind solution $\propto r^{-3/2}$ (eq. [3.10])

$$n_0(r) = \left(\frac{3\Phi_i}{4\pi\alpha_2 r^3}\right)^{1/2} \quad (r \le r_w)\,. \qquad (5.2)$$

The only difference between equation (3.10) and equation (5.2) is that the strong wind case applies to $r \le r_w$ whereas the weak wind case applies to only $r \le r_g$. The underlying reason for this difference involves the attenuation of direct stellar photons penetrating the atmosphere and flow regions. In the case of a weak wind, the atmospheric scale height curves (with positive second derivative) upward out to r_g, where the scale height equals r_g. This means that beyond r_g the effective attenuation

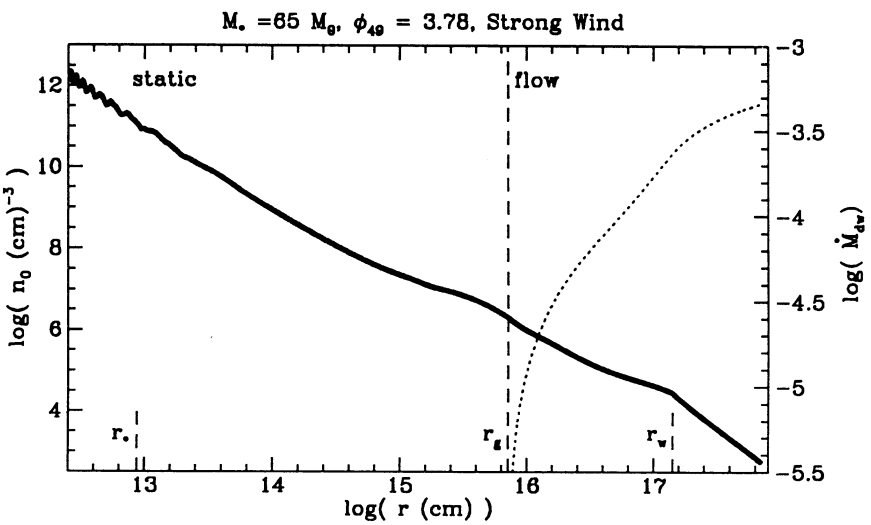

FIG. 9.—Similar numerical solution as in Fig. 3 for a 65 $M_\odot$ star with a strong wind (model 7)

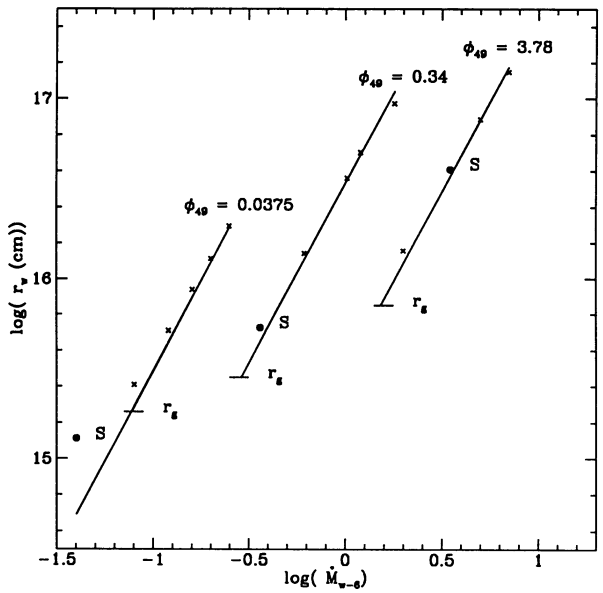

FIG. 10.—Numerical solutions for r_w vs. strength of the stellar wind. The three solid lines show the results of the analytic equation presented in the text (eq. [4.3]) for the three ionizing (stellar masses) cases considered. The short horizontal tick marks indicate the position for r_g for each series "S" denotes the standard wind case; if S lies above the r_g tick marks, then the standard wind lies in the strong wind regime.

pathlength for stellar photons is roughly $r - r_g$, whereas for $r < r_g$ the effective pathlength is a *constant fraction* of r. It is this relative change in the attenuation pathlength which drives $n_0(r)$ from a $r^{-3/2}$ dependence on the inside to a $r^{-5/2}$ dependence on the outside. In the strong wind case, the wind/H II plasma boundary curves upwards more slowly, and it is at r_w where the height of the evaporating H II plasma equals the radius. Therefore, the solution $n_0(r) \propto r^{-3/2}$ persists to r_w, and falls rapidly for $r > r_w$ as the effective attenuation pathlength increases from a constant fraction of r to $r - r_w$.

In essence, the strong stellar wind drives down the atmosphere and allows enhanced penetration of direct stellar photons to greater radii ($r > r_g$) and smaller heights z above the plane. The combination of the direct stellar photons maintaining ionization above the plane, and the diffuse photons produced largely at r_w shining down on the plane and creating the evaporating flux, increases $n_0(r)$ for $r > r_g$, and thereby increases the mass-loss rate from the disk. Most of the mass is now lost at a radius $r \simeq r_w$, and the integrated volume emission measure from the flow peaks at r_w. Equation (4.3) for r_w is derived by equating the ram pressure of the wind to $2n_0(r)kT$, where $n_0(r)$ is taken from equation (5.2) and $T = 10^4$ K. Substituting equation (5.2) for $n_0(r)$ into equation (5.1) for $\dot{M}_{\rm dw}$, we obtain an analytic expression for the evaporative mass-loss rate in the strong wind case:

$$\dot{M}_{\rm dw} \simeq 6 \times 10^{-5} \dot{M}_{w-6} v_{w8} \Phi_{49}^{-1/2} \, M_\odot \, {\rm yr}^{-1} , \qquad (5.3)$$

where the numerical coefficient has been adjusted by a factor of order unity to best fit the numerical results. Note that the analytic expression predicts precisely the numerically determined dependences on $\dot{M}_w$ and Φ_i. Applying the observed correlation of $\dot{M}_w$ to Φ_i given in equation (4.2), we obtain a simpler expression for standard wind models:

$$\dot{M}_{\rm dw} \simeq 6 \times 10^{-5} \Phi_{49}^{0.44} v_{w8} \, M_\odot \, {\rm yr}^{-1} . \qquad (5.4)$$

This latter equation makes it clear that more massive stars generally have greater photoevaporative mass-loss rates from their disks.

6. THE EFFECT OF DUST ON THE PHOTOEVAPORATIVE FLOW

In Appendix A we verify a posteriori that the assumptions of thermal balance, ionization balance, and spatially thin neutral disks are generally valid for typical disks around massive stars. However, our model has also assumed that the effects of dust on the radiative transfer and the gas dynamics can be neglected. This is a marginal assumption, as we will show below, and dust may play an important role in moderating the photoevaporation of disks around massive stars.

Dust grains will sublimate to a distance

$$r_{\rm gr} = 1 \times 10^{15} L_{*5}^{1/2} T_{s3}^{-2} Q_{-1}^{-1/2} \ {\rm cm} , \qquad (6.1)$$

where $L_* = 10^5 L_{*5} \, L_\odot$ is the stellar luminosity, $T_s = 10^3 T_{s3}$ K is the dust sublimation temperature and $Q = 0.1 Q_{-1}$ is the effective absorption efficiency of the dust grains at the sublimation temperature. Therefore, dust may be ignored to $r_{\rm gr} \lesssim r_g$. Beyond $r_{\rm gr}$ the effective column densities $N_{\rm II}$ through which photons must travel at a radius r is given by $N_{\rm II} = r n_0(r)$ or

$$N_{\rm II} = 1.8 \times 10^{22} \Phi_{49}^{1/2} r_{15}^{-1/2} \ {\rm cm}^{-2} , \qquad (6.2)$$

in the critical flow region $r_{\rm gr} < r < r_g < r_g$ or r_w. The evaporating H II gas will entrain the dust that exists at the surface of the neutral disk and carry it along in the flow. If this dust has the standard dust to gas ratio and size distribution of the interstellar medium, the dust will provide an optical depth to Lyman continuum photons of order

$$\tau_{\rm Ly} \sim 30 \Phi_{49}^{1/2} r_{15}^{-1/2} . \qquad (6.3)$$

For the case of massive stars with $\Phi_{49} \sim 0.01$–1, this violates the assumption that dust opacity is negligible and the solutions for $n_0(r)$ and $\dot{M}_{\rm dw}$ need to be scaled down so that $\tau_{\rm Ly} \sim 1$ (i.e., by factors of about $30 \Phi_{49}^{1/2} M_1^{-1/2}$ for the weak wind case and $10 \Phi_{49}^{1/2} r_{w16}^{-1/2}$ for the strong wind case). On the other hand, it seems quite likely that dust will both settle and coagulate in these dense disks, so that the opacity of the dust at the neutral disk surface may be greatly reduced from interstellar values. In addition, the dust may scatter UV photons from the upper atmosphere toward the midplane, an effect that will increase the photoevaporation rate. It is clear that dust opacity is a *potentially* important parameter in controlling evaporative flows from disks around *massive* stars. The results presented in §§ 3 and 5, which ignored dust opacity, can be considered upper limits for $\dot{M}_{\rm dw}$. The lower limit is given by the assumption of ISM grain parameters that, as discussed above, can lower $\dot{M}_{\rm dw}$ by factors of up to 10–$30 \Phi_{49}^{1/2}$.

Entrained dust may also play an important role in the dynamics of the H II gas flow once it evaporates from the disk. Radiation pressure on dust around massive stars can accelerate outflow once $L_* \gtrsim 10^3 \, L_\odot$ (Kahn 1974; Yorke & Krugel 1977; Yorke 1979; Wolfire & Cassinelli 1987). Radiation pressure may also act directly on the gas, via the UV resonance lines. Therefore, not only will thermal gas pressure gradients accelerate the gas and turn the vertical flow into a spherical outflow, but radiation pressure will play a similar role. We anticipate that terminal velocities of $\gtrsim 30$–50 km s^{-1} may be achieved. In this paper we have ignored any such acceleration, assuming it is appreciable only after the evaporating gas has risen in height to $z \sim r$. Our assumption leads to underesti-

mates of $\dot{M}_{dw}$ (by factors of order of the velocity increase, or ~ 3–5), since acceleration will lower the gas densities and allow greater penetration of the Lyman continuum photons that generate the flow. Therefore, the two major effects of dust work in opposite directions in moderating $\dot{M}_w$.

7. APPLICATON TO ULTRACOMPACT H II REGIONS

7.1. *Observations*

Wood & Churchwell (1989a) observed 75 UC H II regions using the VLA at wavelengths of 2 and 6 cm. The angular resolution of these observations was 0".4, or 6×10^{16} cm at 10 kpc. Wood & Churchwell separated their sample into five main morphologies: 43% were spherical or unresolved, 20% were cometary, 17% were irregular or multiply peaked, 16% were core-halo, and 4% had a spherical shell configuration. In the spherical or unresolved category, 19% (or 8% of the entire sample) were unresolved. In the core-halo category, the core diameters at the 50% level are of order 10^{17} cm. The emission measures (averaged over the beam) of the entire sample ranged from $\sim 10^7$ to 10^9 pc cm^{-6}; the emission measure of the unresolved sources were generally $\sim 10^8$ pc cm^{-6}. The inferred average electron densities in the beam range from $\sim 10^4$ to 3×10^5 cm^{-3} for the entire sample; the unresolved regions and cores have electron densities in excess of $\sim 10^5$ cm^{-3}. Wood & Churchwell (1989a) and Kurtz, Churchwell, & Wood (1994) find that the frequency dependence ($L_\nu \propto \nu^{-\alpha}$) between 2 and 6 cm for the unresolved sources in the sample is such that α ranges from 0 to 2, with a mean value (and a large number of individual cases) around 0.6. The large range observed may be indicative that the turnover from optically thin to optically thick emission occurs at $\lambda \sim 2$–6 cm.

The first Wood & Churchwell (1989a) survey covered only a few selective fields of view. The 75 detected UC H II regions in this sparse sampling of the Galactic plane indicate that these regions are longer lived than their dynamical expansion timescales of $\sim 10^4$ yr. However, the second Wood & Churchwell (1989b) survey utilized the *IRAS* PSC and the optical O star counts by Conti et al. (1983) to provide the estimate that perhaps 10%–20% of the main-sequence lifetime of O and B stars (or $\gtrsim 10^5$ yr) is spent in the UC H II stage.

7.2. *Photoevaporation Model of* UC H II *Regions*

7.2.1. *Weak Wind Models*

The weak wind model of photoevaporating disks provides a possible explanation of the *unresolved* UC H II regions. Assuming the existence of a *continuous* thin disk extending to $r \gg r_g$, we showed in § 3 that photoevaporation causes a mass-loss $\dot{M}_{dw}$ from the disk, with most of the mass loss occurring at $r \gtrsim r_g$. Pressure gradients in the initially vertical flow off the disk will convert the flow to a spherically symmetric wind for $r \gg r_g$, with velocity $v_{dw} \sim 10$–50 km s^{-1}. The radio emission from such a flow is optically thick inside of $r < r_{cr}$, where r_{cr} is given by

$$r_{cr} = 7 \times 10^{15} \dot{M}_{dw-5}^{2/3} \left(\frac{\lambda}{3 \text{ cm}}\right)^{0.7} \text{ cm}, \quad (\lambda > \lambda_{min}), \quad (7.1)$$

where $\dot{M}_{dw-5} = \dot{M}_{dw}/10^{-5}\ M_\odot$ yr^{-1} and r_{cr} must be greater than r_g (or $\lambda > \lambda_{min}$) for the flow to be optically thick and for equation (7.1) to apply. The critical wavelength λ_{min} is given as

$$\lambda_{min} = 0.2 M_1^{1.43} \dot{M}_{dw-5}^{-0.95} \text{ cm}. \quad (7.2)$$

Since the density in the ionized flow falls as r^{-2}, the intensity of the radio emission for impact parameters $b > r_{cr}$ drops rapidly away from the central source, as b^{-3}. Thus at $\lambda = 2$ cm (15 GHz) and 6 cm (5 GHz), a $\dot{M}_{dw} = 10^{-5}\ M_\odot$ yr^{-1} source will appear as a relatively constant brightness circle ($T_b \sim 10^4$ K) of radius $r_{2\text{ cm}} \simeq 5 \times 10^{15}$ cm and $r_{6\text{ cm}} \simeq 10^{16}$, with rapidly declining intensity outside the circle. Since the VLA beamsize resolves only those sources with radii greater than $r_{VLA} \simeq 3 \times 10^{16} (D/10 \text{ kpc})$ cm (angular sizes $>0''.4$), where D is the distance to the source, photoevaporating disks around stars with weak winds will be unresolved or marginally resolved at these wavelengths. Therefore the weak wind model generally applies only to the small ($\sim 10\%$) percentage of UC H II regions that are unresolved.

Although we prefer to explain *resolved* UC H II regions with strong wind models, one can envision weak wind solutions that produce more extensive sources. The assumption of a *continuous* thin disk may not be self-consistent. Since the photoevaporative mass loss peaks at $r \sim r_g$ in the weak wind case, this region must be continuously replenished at the rate of photoevaporation or a gap will be produced. If a gap is produced that extends from r_g to r_i, the disk will photoevaporate predominantly from the region just outside the gap, at $r \sim r_i$. Without any attenuation of the diffuse ionizing flux betwen r_g and r_i due to recombining atoms, the mass loss at r_i is now enhanced and the total mass loss from the outer disk becomes

$$\dot{M}_{dw} \simeq 1.3 \times 10^{-5} \left(\frac{M_*}{10\ M_\odot}\right)^{1/2} \left(\frac{r_i}{10^{15} \text{ cm}}\right)^{1/2} \Phi_{49}^{1/2}\ M_\odot \text{ yr}^{-1}, \quad (7.3)$$

assuming $r_i > r_g$. The mass-loss rate *increases* as the gap grows! The integrated emission measure is now dominated by the evaporating flow at r_i, and as the gap grows larger and r_i increases, the source size increases and larger, resolved UC H II regions may be produced.

For the weak wind case with no gap, the predicted emission measure averaged over a 0".4 beam is given:

$$EM \simeq 10^8 \dot{M}_{dw-5}^{4/3} \left(\frac{\lambda}{3 \text{ cm}}\right)^{0.7} \left(\frac{5 \text{ kpc}}{D}\right)^2 \text{ cm}^{-6} \text{ pc}, \quad (\lambda_{min} < \lambda < \lambda_{max}), \quad (7.4)$$

where λ_{max} is defined as the minimum of the following: (1) the wavelength where r_{cr} fills the beam or (2) the wavelength where r_{cr} is equal to the distance at which the flow stops as it encounters the interstellar pressure. By the first criterion

$$\lambda_{max} \simeq 13 \left(\frac{D}{10 \text{ kpc}} \frac{\theta_B}{0''.4}\right)^{1.43} \dot{M}_{dw-5}^{-0.95} \text{ cm}, \quad (7.5)$$

where θ_B is the beam angle. By the second criterion and assuming an interstellar pressure of $P_{ISM}/k = 10^4 p_4$ cm^{-3} K,

$$\lambda_{max} \simeq 4.4 \times 10^4 p_4^{-0.71} \dot{M}_{dw-5}^{-0.24} \text{ cm}. \quad (7.6)$$

Therefore, for unresolved sources, the predicted frequency dependence of L_ν is given by the optically thick, constant velocity wind solution

$$L_\nu \propto \nu^{0.6} \quad (\lambda_{min} < \lambda < \lambda_{max}). \quad (7.7)$$

The unresolved ultracompact H II region around MWC 349A may be the most extensively studied example of the weak wind case of a photoevaporating disk. The central star has been

classified a Be star, although its Lyman continuum luminosity $\Phi_i \gtrsim 10^{48}$ s^{-1} is more appropriate to an O star (Cohen et al. 1985). The observations of masing hydrogen recombination lines in this star (Martin-Pintado et al. 1989a, b; Gordon 1992; Planesas, Martín-Pintado, & Serabyn 1992; Thum, Martín-Pintado, & Bachiller 1992) have been interpreted to arise from a Keplerian disk, at a radius of $r \simeq 20$–30 AU where $n_0 \simeq 10^7$ cm^{-3}. We note that this critical radius is about r_g, and that the weak wind model predicts such a value for n_0 at this radius (eq. [3.11]). The continuum observations from 100 μm to 20 cm reveal a power law $L_\nu \propto \nu^{0.6}$, consistent with an optically thick evaporative flow. The observed $\nu^{0.6}$ dependence extends to shorter wavelength than predicted by equation (7.2), indicating significant flow originating *inside* of r_g. We are currently working on a more exact hydrodynamical calulation of the flow that will determine the flow characteristics inside of r_g. However, it is the observed small upper limit to $\lambda_{\rm min}$ that suggests to us that MWC 349A has a weak *stellar* wind. We will show below the strong stellar winds lead to much higher values of $\lambda_{\rm min}$. The velocity of the outflow has been measured by Altenhoff, Strittmatter, & Wendker (1981) to be of order 25–50 km s^{-1}. Although this velocity is higher than the assumed ~ 10 km s^{-1} flow velocities in our simple model, a more exact hydrodynamical calculation that included the accelerations due to pressure gradients and radiation pressure may provide closer agreement. The inferred mass-loss rate is $\sim 10^{-5}\ M_\odot$ yr^{-1} (Olnon 1975), consistent with the photoevaporative model for $\Phi_{49} \sim 0.1$–1.

7.2.2. *Strong Wind Models*

In the strong wind case, the flow is optically thick only when $\lambda > \lambda_{\rm min}$, where in this case

$$\lambda_{\rm min} \simeq 13(\dot{M}_{w-6}\, v_{w8})^{2.86} \Phi_{49}^{-1.43} \dot{M}_{\rm dw-5}^{-0.95} \text{ cm} . \quad (7.8)$$

The integrated emission measure is dominated by plasma at the origin of the flow (r_w) for $\lambda < \lambda_{\rm min}$; the intensity of the radio emission for impact parameters $b > r_w$ drops rapidly as b^{-3} for $\lambda < \lambda_{\rm min}$. The emission may be resolved by the VLA, and these models may therefore apply to the bulk of the UC H II regions seen in the radio: they are resolved and have sizes $\sim 10^{16}$–10^{17} cm, which is of order of r_w for standard wind parameters.

Assuming the flow is resolved and using the correlation of Φ_i to $\dot{M}_w$ (eq. [4.2]), the peak emission measure in the strong wind case is given as

$$\text{EM} \simeq 10^9 \Phi_{49}^{-0.76} v_{w8}^{-4} \text{ cm}^{-6} \text{ pc} \quad (\lambda < \lambda_{\rm min}) . \quad (7.9)$$

The luminosity will vary as $L_\nu \propto \nu^{-0.1}$ for $\lambda < \lambda_{\rm min}$ and $L_\nu \propto \nu^2$ for $\lambda > \lambda_{\rm max}$. For $\lambda_{\rm min} < \lambda < \lambda_{\rm max}$, $L_\nu \propto \nu^{0.6}$. In the strong wind case, $\lambda_{\rm min} \sim \lambda_{\rm max}$ for the VLA beam size, so that a single beam VLA measurement would detect only a limited range of $\nu^{0.6}$ dependence. However, mapping or the use of larger beams could extend the range of $\nu^{0.6}$ dependence since $\lambda_{\rm max}$ increases with beam size. We therefore predict that mapping UC H II regions to obtain L_ν should uncover an extended range of wavelength $\lambda > \lambda_{\rm min}$ where $L_\nu \propto \nu^{0.6}$. We note that equations (7.4) and (7.9) are upper limits to EM if significant dust is entrained in the flow.

7.2.3. *Brackett Emission*

At sufficiently short wavelengths ($\lambda \ll 1$ mm) the neutral disk becomes optically thick to photons because of the dust opacity. Therefore, in observing high-frequency hydrogen recombination lines such as Brα or Brγ, one only sees the emission from the side of the disk facing the observer. For short wavelengths, $\lambda < \lambda_{\rm min}$, the optically thin emission measure has significant contributions from $r < r_g$, since $n_0(r) \propto r^{-3/2}$. Consequently, the bound, orbiting H II atmosphere will be observed as fairly broad emission, centered on the stellar velocity but extending to nearly the orbital speeds (~ 200 km s^{-1}) of the inner disk, assuming the disk is not perfectly face-on to the observer. However, superposed on this broad pedestal will be the substantial Brackett emission from the outflowing gas at r_g or r_w. Since the neutral disk is optically thick to the Brackett lines, this emission will be blueshifted relative to the central star (or the optically thin radio recombination line emission) by about 10–30 km s^{-1} and will have a line width of similar order.

7.2.4. *Lifetime of* UC H II *Regions*

The UC H II region persists as long as the disk survives the mass loss. For both the weak and strong stellar wind cases, the characteristic lifetime of a photoevaporating disk is given by the mass of the disk divided by the rate of evaporation of the disk, $\tau = M_d/\dot{M}_{\rm dw}$. Using equations (3.14) and (5.4), we get

$$\tau \simeq 7 \times 10^4 \Phi_{49}^{-1/2} M_1^{-1/2} M_d \text{ yr (weak winds)} , \quad (7.10)$$

$$\tau \simeq 2 \times 10^4 \Phi_{49}^{-0.44} v_{w8}\, M_d \text{ yr (strong winds)} , \quad (7.11)$$

if we measure M_d in solar masses. Thus lifetimes of $\gtrsim 10^5$ yr can readily be achieved by 2–10 $M_\odot$ disks. The mass requirement of the disk is reduced by an order of magnitude if the outflows are dusty.

8. SUMMARY

Ultracompact H II regions around massive stars are observed to have much longer lifetimes ($\gtrsim 10^5$ yr) than their dynamical expansion timescales ($\sim 3 \times 10^3$ yr). We propose that many of these regions are maintained by the steady replenishment of the expanding plasma by material photoevaporating from a neutral disk orbiting the young massive star.

The morphology and rate of the photoevaporative flow depends on the strength of the stellar wind. A critical stellar mass-loss rate $\dot{M}_{\rm cr}$ ($\sim 10^{-7} \Phi_{49}^{1/2}\ M_\odot$ yr^{-1}; see eq. [4.1]) is identified. In the weak wind case, $\dot{M}_w < \dot{M}_{\rm cr}$, the ionizing photons from the central star creates a relatively static, $T = 10^4$, ionized atmosphere above the disk out to a critical distance $r_g \sim 10^{15} M_1$ cm. The Lyman continuum flux from the star maintains ionization in the upper atmosphere, while the Lyman continuum photons produced by recombinations to the ground state in the upper atmosphere maintain the ionization at the base of the atmosphere and determine the base electron density $n_0(r)$ (see eq. [3.11]). Beyond r_g, the thermal speed of the 10^4 K gas exceeds the escape velocity from the star/disk system, and an evaporative flow is established with a speed $v_f \gtrsim a \sim 10$ km s^{-1}, the sound speed of the H II plasma. Ultimately, thermal pressure gradients and radiation pressure on dust may accelerate the outflow to terminal speeds of ~ 30–50 km s^{-1}. The evaporative mass-loss rate is found to be $\sim 1 \times 10^{-5} \Phi_{49}^{1/2} M_1^{1/2}\ M_\odot$ yr^{-1} (eq. [3.14]), dominated by particle flux from r_g created by the diffuse photon flux. The optically thick $\lambda \sim 2$–6 cm radio wavelength region extends out to radii of order 10^{16} cm, and this optically thick outflow produces a $L_\nu \propto \nu^{0.6}$ spectrum in the centimeter wavelength region for large beam measurements. The average emission measure in a 0".4 (VLA) beam is of order 10^8 cm^{-6} pc (eq. [7.4]). Weak wind models may apply to stars later than B0 and to O stars with especially weak stellar winds. MWC 349 may

be the best studied example. The unresolved UC H II regions of Wood & Churchwell are potential candidates.

In the strong stellar wind case, $\dot{M}_w > \dot{M}_{cr}$, the ram pressure of the wind sweeps away the bulk of the atmosphere for $r < r_g$. The direct photons from the star penetrate farther and produce larger photoevaporative fluxes of proton-electron pairs from the disk at $r > r_g$. At a critical distance r_w ($> r_g$, see eqs. [4.3] and [4.4]), the thermal pressure of the evaporative flow equals the ram pressure of the wind, and the wind is shocked and deflected out of the plane of the disk. The evaporative mass loss in this case is dominated by the particle flux at r_w, and the mass-loss rate is $\sim 6 \times 10^{-5} \Phi_{49}^{0.44} M_\odot$ yr^{-1} (eq. [5.4]). The UC H II regions formed by these evaporative outflows are likely to be resolvable by the VLA at 2 and 6 cm, and are good candidates for many of the resolved sources of Wood & Churchwell. Their $\lambda = 2$–6 cm emision is likely to be optically thin, $L_\nu \propto \nu^{-0.1}$, with peak emission measures of $\lesssim 10^9$ cm^{-3} (eq. [7.9]).

The frequent occurrence of UC H II regions has long posed a question to astronomers: "Why don't UC H II regions expand and disappear from view in a time much less than their observed lifetime of $\gtrsim 10^5$ years?" In this paper we propose a solution to this paradox: UC H II regions do expand, but the dense ionized gas around the star is replenished for 10^5 yr by material photoevaporating from neutral disks which orbit the young star. Given likely disks masses of $\sim$2–10 $M_\odot$ and disk sizes of $\gtrsim 10^{15}$ cm, we find that the photoevaporative flow persists for $\sim 10^5$ yr in our models. Therefore, UC H II regions may represent the first 10% of the main-sequence lifetime of an O star, as it boils away the remnant accretion disk that once fed its growth.

We thank Ed Churchwell, Mordecai Mac Low, David van Buren, Jack Welch, and Doug Wood for many helpful comments during the course of this work. This research was supported in part by NASA grant RTOP 399-20-01 (Astrophysical Theory Program) which supports the Center for Star Formation Studies, a consortium of theorists from NASA Ames, U.C. Berkeley, and U.C. Santa Cruz. D. J. also acknowledges an NSERC 1967 Fellowship.

APPENDIX A

VERIFICATION OF ASSUMPTIONS

A1. ASSUMPTION OF OPTICALLY THICK, SPATIALLY THIN DISK

We readily verify that the disks around young stars are optically thick to the incident Lyman continuum flux. Assume that the surface density $\Sigma(r)$ of a disk is given by a power law in r

$$\Sigma(r) = \Sigma_d \left(\frac{r}{r_d}\right)^{-\beta}, \tag{A1}$$

where r_d is the outer radius of the disk. Hayashi, Nakazawa, & Nakagawa (1985) used the planet masses in the solar nebular to obtain $\beta = 3/2$ for the disk around the protosun. Constant "α" disks obtain $\beta = 3/4$. We assume for simplicity that $0 < \beta < 2$ and find

$$\Sigma_d = 3.1(2 - \beta) f_{-1} M_1 r_{d16}^{-2} \text{ g cm}^{-2}, \tag{A2}$$

where the disk mass $M_d = 0.1 f_{-1} M_*$ and $r_{d16} = r_d/10^{16}$ cm. The column density of hydrogen through the disk is therefore

$$N(r) = 2 \times 10^{24}(2 - \beta) f_{-1} M_1 r_{d16}^{-2} \left(\frac{r}{r_d}\right)^{-\beta} \text{ cm}^{-2}. \tag{A3}$$

The Lyman flux incident on the disk will penetrate a column

$$N_e(r) \lesssim \frac{\Phi_i}{4\pi r^2 \alpha_2 n_0(r)} N_e(r) \lesssim 7 \times 10^{22} \Phi_{49}^{1/2} r_{15}^{-1/2} \text{ cm}^{-2}, \tag{A4}$$

where the upper limit on the right-hand side of the expression is obtained by ignoring dust attenuation and only including gas attenuation. The disk is thick to Lyman continuum as long as $N_e/N < 1$, or

$$\frac{3 \times 10^{-(2+\beta)}}{(2 - \beta)} \left(\frac{\Phi_{49}^{1/2} r_{15}^{\beta - 1/2} r_{d16}^{2-\beta}}{f_{-1} M_1}\right) < 1. \tag{A5}$$

Note that this condition is readily satisfied for all $r < r_d$ and $0 < \beta < 2$.

The neutral scale height $H_n(r)$ is given by equation (2.2), with $T = T_n$ the temperature of the neutral disk. The neutral disk is heated passively on the surface by the central star and is heated viscously by steady accretion through the disk onto the star. Both processes give $T_n(r) \propto r^{-3/4}$ for the surface (photospheric) temperature of the neutral disk. The latter process deposits heat in the interior of the disk, so that the midplane temperatures are higher than the surface temperatures in order for the heat to diffuse outwards, while in a passively heated disk, the temperature distribution is isothermal in the z direction. Accretion heating can be ignored between the critical radii r_g and r_w if the accretion rate $\dot{M} \lesssim 10^{-4} M_\odot$ yr^{-1}. We use the passively heated solution (Adams, Lada, & Shu 1987)

$$T_n(r) = 2.5 \times 10^4 T_{*4.5} \left(\frac{R_*}{r}\right)^{3/4} \text{ K}, \tag{A6}$$

where $T_{*4.5} = T_*/10^{4.5}$ K is the stellar temperature. In this case,

$$H_n(r) = 6 \times 10^{10} T_{*4.5}^{1/2} R_{*12}^{3/8} M_1^{-1/2} r_{12}^{9/8} \text{ cm} . \quad \text{(A7)}$$

Note that $H_n(r)/r \sim 0.1$ for $r < r_w$. The neutral density at midplane $n_{n0}(r) \sim \Sigma(r)/[m_H H_n(r)]$, or, if $\beta = 3/2$,

$$n_{n0}(r) \sim 5 \times 10^8 \left(\frac{f_{-1} M_1^{3/2}}{r_{d16}^{1/2} R_{*12}^{3/8} T_{*4.5}^{1/2}} \right) r_{16}^{-21/8} \text{ cm}^{-3} . \quad \text{(A8)}$$

Equating the thermal pressure of the H II atmosphere or flow $[2n_0(r)kT]$ to the thermal pressure of the neutral gas at height z_n, we can solve for $z_n(r)$, the height of the neutral gas at radius r. The solution depends on a logarithmic term Λ given by

$$\Lambda = \ln \left(\frac{33 f_{-1} M_1^{3/2} R_{*12}^{3/8} T_{*4.5}^{1/2}}{\Phi_{49}^{1/2} r_{15}^{15/8} r_{d16}^{1/2}} \right) \quad \text{(A9)}$$

$$\frac{z_n}{r} = \frac{0.2 \Lambda^{1/2}}{T_{*4.5}^{1/2} R_{*12}^{3/8} r_{15}^{1/8}} \quad \text{(A10)}$$

Therefore, for the crucial range 10^{13} cm $< r < 10^{16}$ cm, $z_n/r \sim 0.1$–0.4, and the neutral disk is spatially "thin." This calculation ignores the stellar wind, whose ram pressure would make the neutral disk even thinner. Because the diffuse field dominates, the solution for $n_0(r)$ does not depend on the grazing angle of the direct flux with the disk. Therefore, the neutral disk need not be razor thin. Rather, all that is necessary is that there be "room" for roughly one scale height of ionized gas and that the direct flux be able to illuminate the major portion of the ionized atmosphere at r_g. This is equivalent to the condition $z_n/r \lesssim 0.5$. We have numerically found solutions for the case of a constant angle disk surface $z_n/r = 0.4$, and found them to lie within a factor of 1.5 of our infinitely thin disk solutions.

A2. ASSUMPTION OF IONIZATION AND THERMAL EQUILIBRIUM

In the inner regions, $r < r_g$, the electron densities are high, and the timescales to reach ionization and thermal equilibrium are very short compared with the very long dynamical (or "flow") timescales $t_f = r/v_f$. In the evaporating region, $r > r_g$, the dynamical timescales are much smaller and equilibrium may not apply. In this region,

$$t_f = 10^9 M_1 \left(\frac{r}{r_g} \right) \text{ s} , \quad \text{(A11)}$$

where we have assumed that $v_f \sim a \sim 10$ km s^{-1}.

The timescale to achieve ionization equilibrium is given by the recombination timescale $t_i = [n_0(r)\alpha_2]^{-1}$, or

$$t_i = 2 \times 10^5 \Phi_{49}^{-1/2} M_1^{3/2} \left(\frac{r}{r_g} \right)^{3/2} \text{ s} , \quad \text{(A12)}$$

for $r > r_g$ and assuming that $n_0(r) \propto r^{-3/2}$ in the important flow region $r_g < r < r_w$. Ionization equilibrium is valid as long as $t_i < t_f$, or $\Phi_i \gtrsim 4 \times 10^{41} M_1 (r/r_g)$ s^{-1}. Massive stars always fulfill this condition for $r < r_w$. We note, however, that in applying these results to the dispersal of the solar nebula, where $\Phi_i \lesssim 10^{41}$ s^{-1}, this assumption could break down (Shu, Johnstone, & Hollenbach 1993).

We have also implicitly assumed that in the H II atmosphere or flow region above the disk, the gas is mostly ionized (the neutral fraction $x_H \ll 1$). Equating photoionization to recombination, we obtain in the $n_0(r) \propto r^{-3/2}$ region

$$x_H = 1.2 \times 10^{-6} \Phi_{49}^{-1/2} M_1^{1/2} \left(\frac{r}{r_g} \right)^{1/2} . \quad \text{(A13)}$$

Therefore, the assumption $x_H \ll 1$ is valid in the H II regions of the disks of massive stars.

The timescale for thermal equilibrium is approximately $t_c \sim (T/T_*)t_i$, since the heating and cooling rate is proportional to the recombination rate and the heat input per recombination is of order $3kT_*/2$. With $T/T_* \sim 0.2$–0.5 it therefore holds that ionization equilibrium ensures thermal equilibrium. We note that the nonequilibrium condition $t_f < t_c$ is equivalent to the statement that adiabatic cooling of the expanding flow is dominant so that the H II gas will cool to $T \ll 10^4$ K.

REFERENCES

Adams, F. C., Lada, C. J., & Shu, F. H. 1987, ApJ, 312, 788
Altenhoff, W. J., Strittmatter, P. A., & Wendker, H. J. 1981, A&A, 93, 48
Bally, J., & Scoville, N. Z. 1982, ApJ, 255, 497
Beckwith, S. V. W., & Sargent, A. I. 1993, ApJ, submitted
Beckwith, S. V. W., Sargent, A. I., Chini, R. S., & Güsten, R. 1990, AJ, 99, 924
Bloemhof, E. E., Reid, M., & Moran, J. M. 1993, ApJ, submitted
Bodenheimer, P., Yorke, H., & Laughlin, G. 1993, in preparation
Boss, A., & Tscharnuter, J. 1993, in Protostars and Planets III, ed. E. H. Levy & J. I. Lunine (Tucson: Univ. Arizona Press), in press
Cassen, P., & Moosman, A. 1981, Icarus, 48, 353
Cohen, M., Bieging, J. H., Dreher, J. W., & Welch, W. J. 1985, ApJ, 292, 249
Conti, P. S., Garmany, C. D., de Loore, C., & Vanbeveren, D. 1983, ApJ, 274, 302
Edwards, S., Cabrit, S., Strom, S. E., Heyer, I., Strom, K. M., & Anderson, E. 1987, ApJ, 321, 473
Gordon, M. 1992, ApJ, 387, 701
Hartmann, L., Kenyon, S. J., & Calvet, N. 1993, ApJ, 407, 419
Hartmann, L. W., & Raymond, J. C. 1989, ApJ, 337, 903
Hayashi, C., Nakazawa, K., & Nakagawa, Y. 1985, Protostars and Planets II, ed. D. C. Black & M. S. Matthews (Tucson, Univ. Arizona Press), 1100
Hillenbrand, L. A., Strom, S. E., Keene, J., & Vrba, F. J. 1992, ApJ, 397, 613
Kahn, F. D. 1974, A&A, 37, 149
Keto, E., Welch, W. J., Reid, M., Ho, P., & Carral, P. 1993, in preparation
Kurtz, S., Churchwell, E., & Wood, D. O. S. 1994, ApJS, 91, 659
Maeder, A., & Meynet, G. 1987, A&A, 182, 243
Martín-Pintado, J., Bachiller, R., Thum, C., & Walmsley, M. 1989a, A&A, 215, L13
Martín-Pintado, J., Thum, C., & Bachiller, R. 1989b, A&A, 222, L9
Myers, P. C., Heyer, M., Snell, R. L., & Goldsmith, P. F. 1988, ApJ, 324, 907
Olnon, F. M. 1975, A&A, 39, 217

Panagia, N. 1973, AJ, 78, 929
Planesas, P., Martín-Pintado, J., & Serabyn, E. 1992, ApJ, 386, L23
Pottasch, S. R., Wesselius, P. R., & van Duinen, R. J. 1979, A&A, 77, 189
Reid, M. J., Haschick, A. D., Burke, B. F., Moran, J. M., Johnston, K. J., & Swenson, G. W., Jr. 1981, ApJ, 239, 89
Shu, F., Johnstone, D., & Hollenbach, D. 1993, Icarus, submitted
Shu, F., Tremaine, S., Adams, F., & Ruden, S. 1990, ApJ, 358, 495
Tatematsu, K., et al. 1993, ApJ, 404, 643
Tenorio-Tagle, G. 1979, A&A, 71, 59
Terebey, S., Shu, F. H., & Cassen, P. 1984, ApJ, 286, 529
Thum, C., Martín-Pintado, J., & Bachiller, R. 1992, A&A, 256, 507
van Buren, D. 1985, ApJ, 294, 567
van Buren, D., & Mac Low, M.-M. 1992, ApJ, 394, 534
van Buren, D., Mac Low, M.-M., Wood, D. O. S., & Churchwell, E. 1990, ApJ, 353, 570
Wolfire, M. G., & Cassinelli, J. P. 1987, ApJ, 319, 850
Wood, D. O. S., & Churchwell, E. 1989a, ApJS, 69, 831
———. 1989b, ApJ, 340, 265
Yorke, H. W. 1979, A&A, 80, 308
———. 1993, in Massive Stars: Their Lives in the Interstellar Medium, ed. J. P. Cassinelli & E. B. Churchwell (San Francisco: ASP), 45
York, H. S., & Krugel, E. 1977, A&A, 54, 183
Yorke, H. W., Tenorio-Tagle, G., & Bodenheimer, P. 1983, A&A, 127, 313
Yorke, H. W., & Welz, A. 1993, in Star Forming Galaxies and Their Interstellar Media, in press